Supporting Information

Liu et al. 10.1073/pnas.1407229111

SI Text

1. Single Forcing Experiments. The four sensitivity experiments in the Community Climate System Model 3 (CCSM3) [orbital (ORB), greenhouse gas (GHG), meltwater flux (MWF), and ice sheet (ICE)] (Fig. 2*A*), are all initialized from the state of the full forcing CCSM3 transient simulation near the Last Glacial Maximum (19 ka). Each experiment is then integrated with only a single forcing varying with time as in the full forcing experiment (the ORB, GHG, MWF, and continental ice sheet in ICE), whereas other forcings are all prescribed at the value of 19 ka. More details of these sensitivity experiments can be found in a study by He et al. (1). In the Loch-Vecode-Ecbilt-Clio-Agism Model (LOVECLIM) (Fig. 2*B*) and Fast Met Office/UK Universities Simulator (FAMOUS) (Fig. 2*C*), the sensitivity experiments (ORB, GHG, and ICE) are performed similar to those in the CCSM3. It is interesting that the sum of the global temperature of the individual single forcing runs roughly equals that of the full forcing run; this reflects that the global annual mean temperature response to various forcings can be considered largely as a linear sum of the responses to each individual forcing. However, one should note that the difference of the sum from the full forcing experiment is not necessarily caused by nonlinearity. This is because all of the individual forcing runs are started from the glacial state, except for one individual forcing.

The GHG experiment gives an equivalent sensitivity of ∼0.5 °C for a 10% (20 ppm/200 ppm) increase of the equivalent CO_2. This sensitivity is consistent with the state-of-art Intergovernmental Panel of Climate Change models, which show an ensemble mean warming of 3.2 °C in response to a doubling (100% increase) of CO_2 (2). This sensitivity appears 40% higher than that for the present climate in the CCSM3 (2.7 °C) (2). This higher sensitivity occurred because the GHG forcing run was performed on the Last Glacial Maximum (LGM) climate setting, notably with the LGM continental ice sheet boundary condition. We have performed two CO_2 doubling sensitivity experiments with the model settings at the present and LGM states, respectively. The experiments indeed show a 40% stronger model CO_2 sensitivity in the LGM state than in the present state. The enhanced sensitivity at the glacial state is caused mainly by the larger ice sheet cover in the LMG setting, which leads to a colder climate and more snow and sea ice cover, and, in turn, to stronger climate feedback and climate sensitivity.

2. Seasonally Biased Stack. The seasonal biases of the proxies are designed. We used the dataset of Marcott et al. (M13 in ref. 3) because it is a comprehensive compilation selected by M13 using a criterion of sufficient resolution and uncertainty for the purpose of reconstruction of the transient Holocene climate (3). Our seasonally biased scheme is illustrated using different markers for different proxy types in Fig. S1, with the edge color representing the selected season and the face color denoting the temperature trend in the proxy during the Holocene. Following a suggestion by Leduc et al. (4), the alkenone-based and Mg/Ca-based sea surface temperatures (SSTs) in the Northern Hemisphere are assumed to be biased toward the boreal summer. Other sites are unbiased as annual mean or biased toward the local seasons as suggested by Marcott et al. (M13 in table S1 in ref. 3). After determining the seasonal bias at each site, we replace the annual mean value with the corresponding value of the biased season, and then follow the same spatial average scheme as the site-stacked global mean surface temperature to produce the site-stacked seasonally biased time series shown in Fig. 1 (red). The biased stack reverses the annual mean warming (Fig. 1, yellow) to a cooling trend (Fig. 1, red) similar to the M13 reconstruction, but with a magnitude (0.25 °C) about half of that in M13. A test with several alternative schemes shows that this cooling trend in the biased stack is generated mainly by the summer seasonal bias of the alkenone-based SSTs in the Northern Hemisphere. When these SSTs are replaced by their annual mean SSTs, the simulated cooling trend is reversed back to a warming trend similar to the model annual warming (Fig. S2, dark to light green). In comparison, when the tropical alkenone-based SSTs are replaced by their annual means, the global stack still exhibits a cooling trend as in the biased stack (Fig. S2, orange to red).

In M13, a similar analysis was performed on the Holocene part of a LOVECLIM simulation forced by the full forcing (without meltwater), which is similar to our full forcing LOVECLIM simulation (Fig. 1*A*), except all of the forcings in their simulation are accelerated 10-fold (5). Similar global temperature trends were produced in M13 as in our study in both cases with and without the seasonal biases (figure S8 in ref. 5): The global annual temperature shows a warming trend, whereas the seasonally biased temperature shows a cooling trend. Nevertheless, the interpretation of Timm and Timmerman (5) was that "The seasonally biased model stack tends to overrepresent an Early Holocene warming in the modeled mean-annual temperature by 0.25 °C, but the two stacks are otherwise quite similar." This leaves the impression that the M13 reconstruction is not affected significantly by seasonal biases. Here, as discussed in the main text, we interpret the different trends between the annual mean and seasonally biased global temperatures in the model as being significant. To show more clearly the significance of this cooling trend in the biased model stack, we compare the data and model in the Holocene only for the period before 1 ka (Fig. 3); the cooling in the M13 reconstruction after 1 ka could have been reproduced in the transient simulations by imposing the additional forcing of volcanic aerosol and solar variability (Fig. 1, *Inset*). From the Early Holocene to 1 ka, the global temperature cools by ∼0.25 °C in the model, which is about half of the ∼0.5 °C cooling in M13 (Fig. 3*A*). A further observation of the temperature evolution in different regions (Fig. 3 *B*–*D*) suggests that, for the Northern Hemisphere, the model-biased stack cools by ∼1 °C, comparable to that in M13 (Fig. 3*B*). The weaker global cooling in the model is caused mainly by the Southern Hemisphere stack in the model, which shows an annual mean warming, opposite from the early cooling in M13 (Fig. 3*D*). This discrepancy could not be explained by a (austral) summer bias as in the Northern Hemisphere, because the direct insolation effect will not generate a large cooling trend in austral summer. Therefore, this discrepancy may be attributed to potential deficiencies in both the model and the reconstruction. For the reconstruction, there are only nine sites in the Southern Hemisphere stack with limited spatial distribution, which may lead to a sampling error in the estimation of the hemispheric temperature, although we do note that the different climate records consistently show Early- to Mid-Holocene cooling. Alternatively, the models may be missing climate feedbacks related to high-latitude orbitally driven radiative forcing.

3. Regional Model Data Comparison. A brief discussion of model-data comparison on a site-by-site basis also helps us to understand the global mean comparison. Fig. S1 *A*–*C* (background shading) shows, respectively, the Holocene model temperature trend for

annual mean, boreal summer, and boreal winter forced by the full forcing in the ensemble mean of the CCSM3 and FAMOUS (the seasonal data for the LOVECLIM was not available when this study was prepared). For the annual mean, the model shows a warming trend over the entire globe except over the Arctic Ocean (Fig. S1*A*), and therefore significant warming in the global annual mean temperature (Figs. 1 and 3). The boreal summer temperature (Fig. S1*B*) shows a cooling over most of the continental regions and parts of the Northern Hemisphere oceans, which is nevertheless largely canceled in the annual balance by the strong warming in the boreal winter (Fig. S1*C*). A comparison of the trend in the model with the proxies (face color of the markers in Fig. S1) shows little consistency for annual mean and other seasons. The spatial correlations of the temperature trends across the 73 sites between the data and the model are −0.16, −0.03, −0.27, −0.27, and 0.01 for the annual, March–April–May (MAM), June–July–August (JJA), September–October–November (SON), December–January–February (DJF) and biased model stack, respectively (Table S1), reflecting the lack of correlation, even after the potential seasonal bias in the proxies is considered. This can be seen more clearly in the scatter diagram of the reconstruction and model (Fig. 3). Overall, the warming trends in most of the sites in the annual mean case (Fig. S4*A*) are changed to cooling trends in the biased stack, mostly because of the summer bias of alkenone-based SSTs (Fig. S4*B*); however, there is no improvement in the correspondence between the reconstruction and model from the annual mean to the biased stack across sites.

The warming effect of GHGs and ice sheets can be discerned by comparing the temperature trend under the full forcing (Fig. S1 *A*–*C*) and the orbital forcing alone (ORB; Fig. S1 *D*–*F*). With the orbital forcing alone, the region of annual cooling expands significantly into midlatitude at the expense of the warming region at low latitudes. This pattern of temperature response is qualitatively consistent with the annual mean insolation change associated with the decrease of obliquity (6). The increased area of cooling in the Northern Hemisphere helps to reduce some data-model discrepancy at regional scales. The spatial correlations between the data and ORB across the 73 sites are 0.25, 0.21, −0.01, −0.01, and 0.22 for annual, MAM, JJA, SON, DJF, and biased model stack, respectively (Table S1). Now, the data have a significant positive correlation with either the annual mean or the seasonal stack because of the increased cooling trend in the mid- and high latitudes, as seen in the scatter diagram for the annual mean (Fig. S4*C*) and biased stack (Fig. S4*D*). This implies a deterioration of the site-by-site model data discrepancy due to the additional GHG and ice sheet forcing, compared with the orbital forcing alone in previous studies (7). Therefore, the annual warming induced by the GHGs and ice sheets contributes significantly to the discrepancy between the data and model for both the global mean and regional temperatures.

It is interesting to notice that, despite the symmetrical annual mean insolation change of obliquity change, the annual mean cooling is much stronger in the Northern Hemisphere than in the Southern Hemisphere (Fig. S1 *D*–*F*). This hemispherically asymmetrical annual cooling can be understood as the nonlinear SST response to the seasonal precession forcing (8). For ease of thinking, consider the Early Holocene relative to the Late Holocene in the Arctic Ocean; the enhanced seasonal cycle of insolation gives an equal amount of insolation decrease in winter and insolation increase in summer. However, the resultant decrease of the winter SST will be less than the increase in the summer SST, because the former is weakened by the deeper mixed layer and is constrained by the lower bound of the freezing point in the winter. As such, the enhanced seasonal cycle of insolation will lead to an annual mean warming in the Northern Hemisphere, which reinforces the warming in response to the obliquity forcing. Conversely, the decreased seasonal cycle of insolation in the Southern Hemisphere will lead to an annual mean cooling, which reduces the mean warming forced by the obliquity forcing. Therefore, from the Early Holocene to the Late Holocene, the orbital forcing drives a much stronger annual cooling trend in the high latitudes of the Northern Hemisphere than in the Southern Hemisphere (Fig. S1*D*). This cooling in the Arctic is so strong because of the much larger increase of seasonal cycle in response to albedo feedback in the high-latitude region (6), such that it remains a cooling even after the warming by the rising GHGs and retreating ice sheets (Fig. S1*A*).

4. Paleoclimate Modeling Intercomparison Project 6-ka Experiments. The time-slice sensitivity experiments are performed at 6 ka and 0 ka, which are forced by the same forcing, except for the orbital forcing. The models include 15 PIMP2 models (CCSM3, CSIRO-Mk3L-1.0, CSIRO-Mk3L-1.1, LOVECLIMCLIVOECODE, ECHAM5-MPIOM, FGOALS-1.0g, FOAM, GISSmodelE, IPSL-CM4-V1-MR, MIROC3.2, MRI-CGCM2.3.4nfa, MRI-CGCM2.3.4fa, UBRIS-HadCM3M2, BCC-CSM1-1, and GISS-E2-R) and 13 PIMP3 models (CCSM4, CNRM-CM5, HadGEM2-ES, HadGEM2-CC, CSIRO-Mk3-6-0, IPSL-CM5A-LR, CSIRO-Mk3L-1-2, MIROC-ESM, EC-EARTH-2-2, MPI-ESM-P, FGOALS-g2, MRI-CGCM3, and FGOALS-s2).

1. He F, et al. (2013) Northern Hemisphere forcing of Southern Hemisphere climate during the last deglaciation. *Nature* 494(7435):81–85.
2. Randall D, et al. (2007) Climate models and their evaluation. *Climate Change 2007: The Physical Science Basis. Fourth Assessment Report IPCC*, eds Solomon S, et al. (Cambridge Univ Press, Cambridge, UK), pp 589–662.
3. Marcott SA, Shakun JD, Clark PU, Mix AC (2013) A reconstruction of regional and global temperature for the past 11,300 years. *Science* 339(6124):1198–1201.
4. Leduc G, Schneider R, Kim J-H, Lohmann G (2010) Holocene and Eemian sea surface temperature trends as revealed by alkenone and Mg/Ca paleothermometry. *Quat Sci Rev* 29:989–1004.
5. Timm O, Timmerman A (2007) Simulation of the last 21,000 years using accelerated transient boundary conditions. *J Clim* 20:4377–4401.
6. Liu Z, Brady E, Lynch-Steiglitz J (2003) Global ocean response to orbital forcing in the Holocene. *Paleoceanography* 18:1041–1061.
7. Lohmann G, Pfeiffer M, Laepple T, Leduc G, Kim J-H (2013) A model-data comparison of the Holocene global surface temperature evolution. *Climate of the Past* 9: 1807–1839.
8. Erb M, Broccoli A, Clement A (2013) The contribution of radiative feedbacks to orbitally driven climate change. *J Clim* 26:5897–5914.

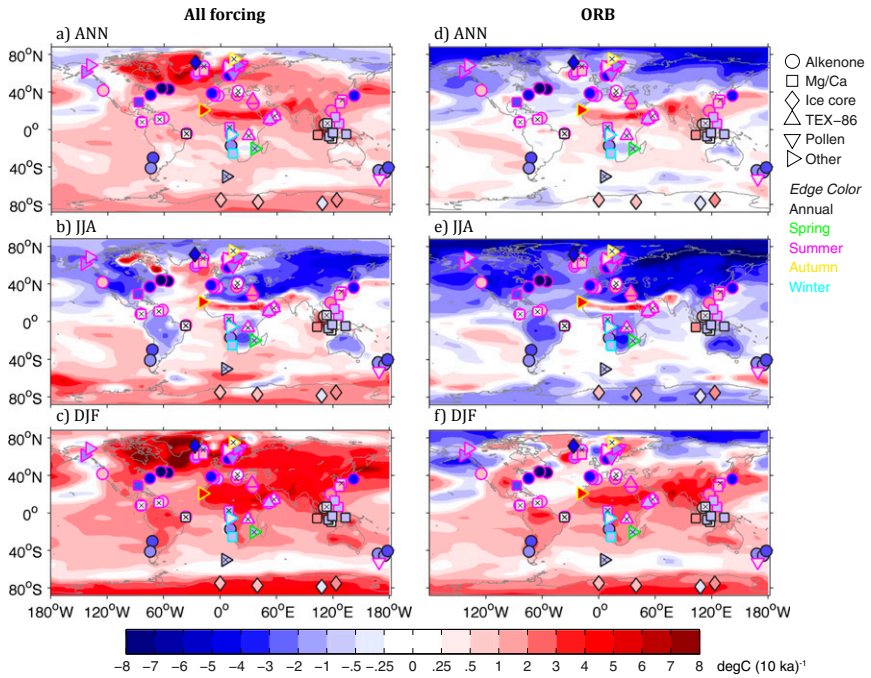

Fig. S1. Model ensemble mean (CCSM3 and FAMOUS) temperature trend (shading) in the Holocene for the all forcing run (*A*–*C*) and ORB (*D*–*F*) simulations for the annual (ANN) mean (*A* and *D*), JJA (*B* and *E*), and DJF (*C* and *F*). The locations of the 73 M13 sites, proxy types (markers), and their temperature trends (from 9 to 0.2 ka, face color of markers) are also plotted as markers in each panel. The assumed seasonal biased stack is denoted by the edge color of the marker: Black is for no seasonal bias or annual mean surface temperature; green, red, yellow, and blue represent the model proxies biased toward local spring, summer, autumn, and winter, respectively. The corresponding sites are indicated using alkenone (○), Mg/Ca (□), ice core (◇), tetraether index of 86 carbon atoms (TEX-86) (△), and pollen (▽), respectively. Right-pointing triangles denote the sites using other proxies. A black "x" indicates the trend is not significant at the 90% level. Readers are referred to table S1 of M13 (3) for details on the proxy records.

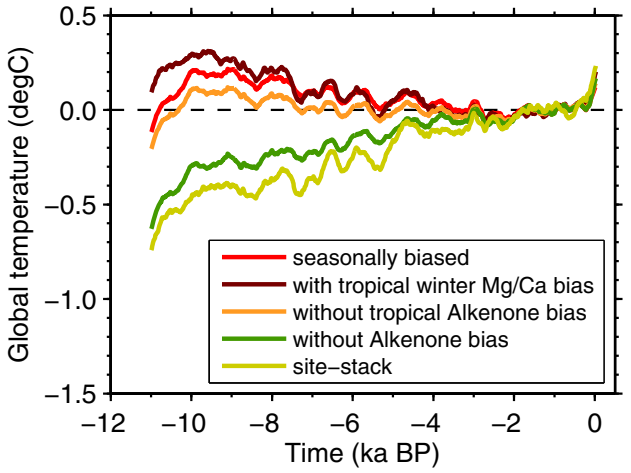

Fig. S2. Site-stack averaged temperature evolution throughout the Holocene from the model ensemble mean (CCSM3, FAMOUS, and LOVECLIM) for five different bias schemes, the annual mean temperature (yellow), the seasonally biased stack as in Fig. S1 (red), and three sensitivity schemes modified on the seasonally biased schemes: All alkenone-based SSTs (25 sites; Fig. S1, purple circles) replaced by the annual mean (dark green), only tropical alkenone-based SSTs (nine sites; Fig. S1, purple circles between 30° S and 30° N) replaced by the annual mean (orange), and the Ma/Ca-based SSTs in the southern tropics (six sites; Fig. S1, black squares between 30° S and 0°) are replaced with local winter (JJA) temperature (dark red). It is seen that the global cooling trend in the biased stack is mainly caused by the assumed summer bias in the alkenone sites in the Northern Hemisphere.

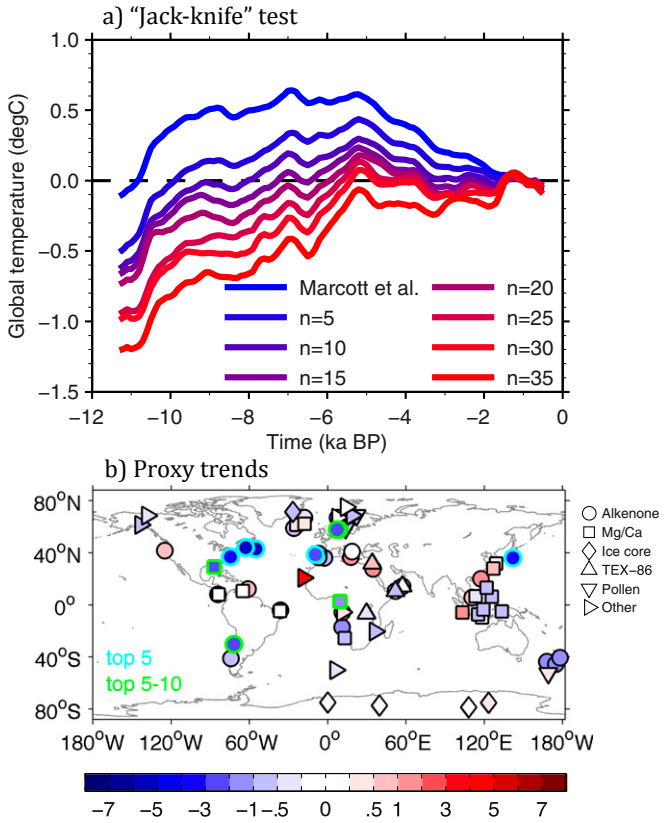

Fig. S3. "Jack-knife" test of the global temperature of the M13 proxy stack. (*A*) Global temperature after removing the top 5, 10, . . .35 sites of the strongest cooling trend in the stack. (*B*) Temperature sites with proxy types and temperature trends in different markers and face colors (the same as in Fig. S1). The top 5 and 10 sites of the largest cooling trends are marked by cyan and green edges, respectively. The top five coolings are all alkenone-based SSTs in the Northern Hemisphere as shown in *B*. Removal of these sites leads to no net cooling from the Early Holocene to the Late Holocene as shown in *A*, although the cooling after the Mid-Holocene is still robust. The pattern remains qualitatively similar, but with a progressive reduction of the cooling trend when more top cooling sites are removed.

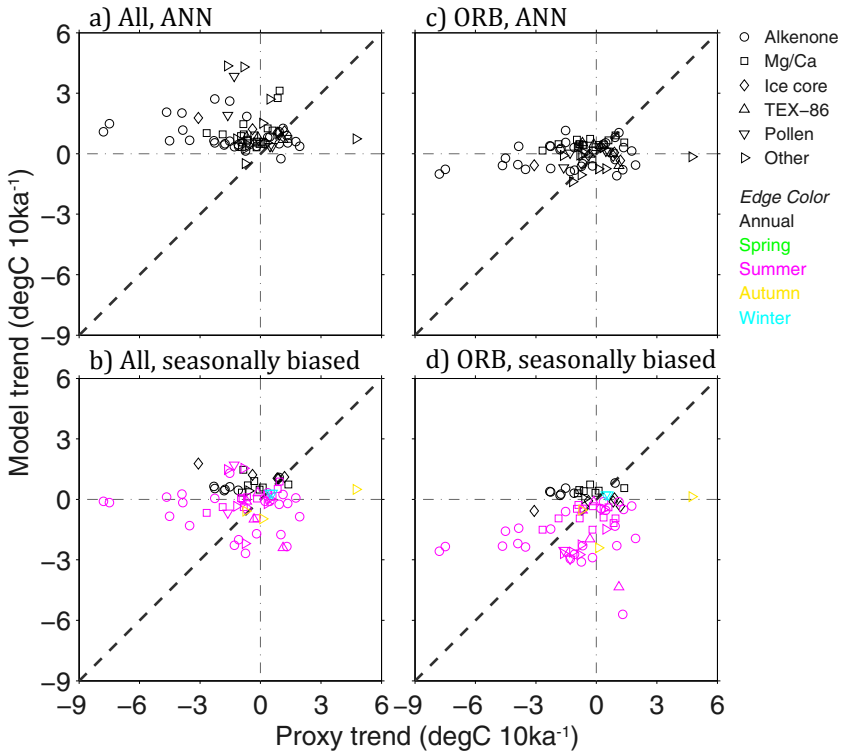

Fig. S4. Scatter plot of the Holocene temperature trends at the 73 M13 stack sites between the reconstruction and model annual mean (*A*) and model seasonally biased stack (*B*) in the transient simulations forced by the full forcing for the model ensemble mean of the CCSM3, FAMOUS, and LOVECLIM. (*C* and *D*) Same as in *A* and *B*, respectively, but for the simulations forced by the orbital forcing only in ORB. The marker for each site is the same as in Fig. S1. For both the full forcing run and ORB run, the seasonally biased stack shifts the trend toward cooling but does not lead to a significant increase of positive correlation with the data trend (correlations similar to that in Table S1 for the ensemble of CCSM3 and FAMOUS). This suggests that the seasonally biased stack is still unable to improve model-data discrepancy at regional scales significantly, although it reduces the global mean model-data discrepancy, with both showing a predominantly cooling trend.

Table S1. Spatial correlation of the temperature trend between the M13 stack and the model for annual mean, MAM, JJA, SON, DJF, and seasonally biased model stack

Spatial correlation of trend	ANN	MAM	JJA	SON	DJF
Ensemble ALL	−0.16 (0.18)	0.03 (0.80)	−0.27 (0.02)	−0.27 (0.02)	−0.10 (0.42)
Ensemble ORB	0.25 (0.03)	0.21 (0.08)	−0.01 (0.92)	−0.01 (0.91)	0.21 (0.07)
Ensemble ALL, seasonally biased	0.01 (0.96)	—	—	—	—
Ensemble ORB, seasonally biased	0.22 (0.06)	—	—	—	—

The term "ALL" refers to the transient simulations with all forcing, whereas the term "ORB" refers to simulations with orbital forcing alone. The ensemble represents the mean of the CCSM3 and FAMOUS. *P* values are shown in parentheses.